THE JOURNAL OF PHYSICAL CHEMISTRY C

pubs.acs.org/JPCC Article

Anharmonic Effects in Single-Walled Carbon Nanotubes Analyzed through Low-Temperature Raman Imaging

Takayuki Umakoshi,[§] Masaki Taniguchi,[§] and Prabhat Verma*

Cite This: J. Phys. Chem. C 2020, 124, 6922–6928 Read Online

ACCESS | Metrics & More | Article Recommendations | Supporting Information

ABSTRACT: The high thermal conductivity of single-walled carbon nanotubes (SWCNTs) has gained much attention for their applications in potential thermal devices. Here, we investigate anharmonic effects, originated from phonon interactions, of SWCNT bundles by temperature dependent Raman imaging using our home-built mini cryostat system. The cryostat system is small enough to be mounted on a piezo scanner that suppresses thermal drift, enabling Raman imaging at different temperatures. We obtained Raman spectral images of several SWCNT bundles with a spatial resolution of a few hundred nanometers at different temperatures. We found that different bundles show different temperature dependences of Raman peak intensity, shift, and width. The temperature dependence was further elucidated by considering the sample topography observed by atomic force microscopy, where bundle effects seem to play an important role to influence the anharmonicity. The temperature-dependent Raman analysis based on spatially resolved imaging will be a powerful tool to investigate anharmonic effects of advanced carbon nanomaterials as well as to realize in situ visualization of thermal properties for future thermal devices.

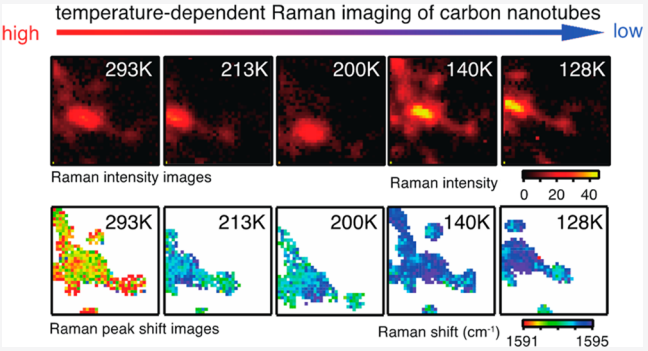

Downloaded via OSAKA UNIV on April 2, 2020 at 02:43:04 (UTC).
See https://pubs.acs.org/sharingguidelines for options on how to legitimately share published articles.

1. INTRODUCTION

Single-walled carbon nanotubes (SWCNTs) have been extensively studied over decades as a promising nanomaterial owing to their remarkable electrical, optical, and thermal properties.[1−3] These one-dimensional structures with extremely high aspect ratios also provide unique mechanical properties.[4] In particular, the extremely high thermal conductivity along the tube axis has recently been identified to be of great importance, as it can contribute to future thermal devices as a heat conductor.[3,5] To characterize such thermal properties of SWCNTs, temperature-dependent Raman spectroscopy has often been utilized. Raman spectroscopy is a powerful analytical technique that can invasively evaluate phonon vibrations of samples,[6−11] and SWCNTs exhibit representative Raman scattering peaks such as the G^+-band, the G^--band, the D-band, and the radial breathing mode (RBM).[12] The peak position and the peak width of Raman modes vary with temperature. For instance, as the temperature of SWCNTs rises, the peak intensity of the G^+-band decreases, the peak width increases, and the peak position redshifts, which can be explained by the anharmonicity in the vibrational potential of the G^+-band that leads to the decay of strongly interacting optical phonons (G^+-band) into weakly interacting acoustic phonons. The acoustic phonons recombine back into optical phonons, giving rise to a cubic or higher order anharmonicity.[6−8] These anharmonic effects originating from phonon interactions become prominent at higher temperatures.[13,14] It is therefore possible to investigate the anharmonicity in SWCNTs by measuring Raman scattering at different temperatures. The temperature-dependent Raman scattering has been evaluated in different forms of SWCNT samples such as bundled SWCNTs on a substrate, isolated suspended SWCNTs, or even during the growth stage of SWCNTs.[15−19]

However, temperature-dependent Raman measurements of SWCNTs are mostly performed at temperatures higher than the room temperature, going up to around 1000 K, and Raman spectra of SWCNTs at low temperatures have rarely been studied so far. Although a few reports have shown Raman spectra at low temperatures, they mostly compared Raman spectra only between two temperatures—the room temperature and the liquid helium temperature (4 K),[16,20] where no spectral dependence was evaluated at temperatures in between. The changes in Raman spectrum at high temperatures are simple and nearly proportional to the temperature; however, it behaves in a complicated way at low temperatures due to a

Received: January 15, 2020
Revised: March 1, 2020
Published: March 4, 2020

ACS Publications © 2020 American Chemical Society

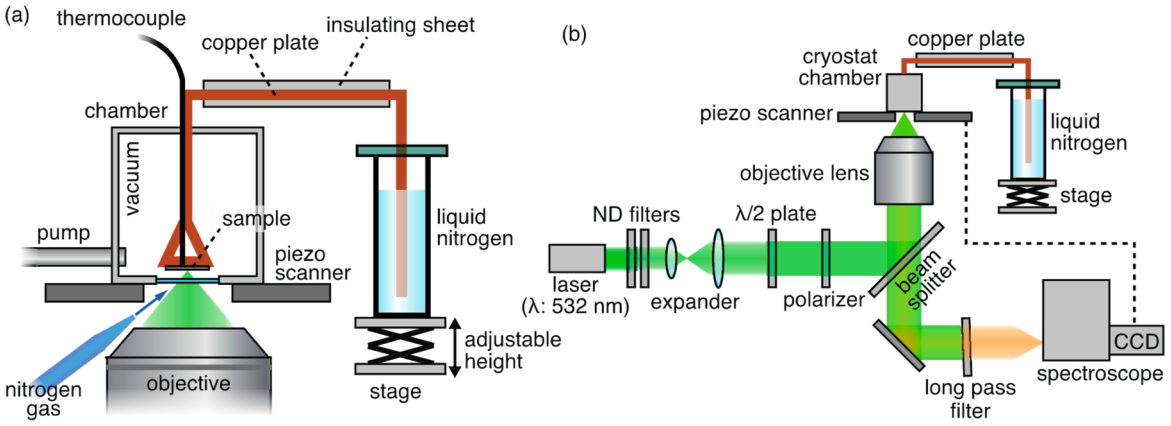

Figure 1. (a) Schematic of the home-built cryostat system. (b) Schematic of the experimental setup.

complex change in the anharmonic components, as will be discussed in detail later. It is therefore difficult to completely understand the anharmonicity at low temperatures; however, this understanding is significantly important for future applications.

Moreover, only one-point measurements have been demonstrated for the temperature-dependent Raman analysis of carbon nanotubes for both low and high temperatures, and no spatially resolved Raman imaging analysis has been reported so far.[13−19,21,22] It is mostly because a sample drift often occurs due to the thermal expansion of the sample stage when the temperature is changed. A small sample drift can happen even when one tries to maintain the temperature constant. This is a crucial issue especially for Raman imaging because such a slow imaging technique requires at least a few minutes for one image to acquire intrinsically weak Raman signals from multiple points. Thus, Raman measurements are usually compromised by obtaining spatially averaged information from multiple SWCNT samples to avoid artifacts due to the thermal drift. However, temperature-dependent analysis of SWCNTs based on Raman imaging is expected to give a much deeper insight into understanding detailed thermal properties of individual SWCNT samples. The thermal properties of SWCNTs depend on many factors, such as their configurations and surrounding atmosphere. Raman-imaging-based analysis can visualize such differences in individual SWCNTs, which could be buried in spatially averaged information from multiple SWCNTs. It would also become a powerful tool for in situ visualization of the thermal properties in actual thermal devices with a spatial resolution of a few hundred nanometers.

In this study, we demonstrate temperature-dependent Raman imaging analysis of SWCNT bundles to study the anharmonicity of phonon vibrations in individual SWCNT bundles, using our home-built cryostat that is compatible for Raman imaging at low temperatures. We constructed a cryostat composed of some simple parts to suppress the thermal drift. This home-built cryostat is small enough to be mounted on a piezo scanner, and it includes a glass window for optical access. The design of our cryostat enables Raman spectral imaging at low temperatures. Through Raman imaging of several SWCNT bundles at various temperatures, we found different behaviors of Raman spectra and anharmonicity for different SWCNT bundles. The Raman spectra obtained at various temperatures were further elucidated by considering the topographic structures of each SWCNT bundle observed by atomic force microscopy (AFM), in which we reveal the significance of bundle effects to the anharmonicity in SWCNT bundles.

2. EXPERIMENTAL SECTION

Figure 1 illustrates the schematics of the experimental setup together with the details of the cryostat that we constructed. We used a cylindrical plastic chamber with a diameter of around 30 mm and a height of around 50 mm. Although ordinary cryostat systems directly flow liquid nitrogen into the sample holder through a tube, we separated cooling medium of liquid nitrogen from the sample chamber to make the entire chamber system simple and small, as shown in Figure 1a. We inserted a copper plate as an efficient heat conductor into the chamber, one end of which was in physical contact with the sample stage to reduce the temperature of the sample. The other end of the copper plate was dipped in liquid nitrogen so that the temperature of the sample could be efficiently reduced by transferring heat along the plate to liquid nitrogen. In order to facilitate an efficient reduction of temperature, we covered the middle part of the copper plate with an insulating sheet. The temperature was controlled from 123 K to room temperature (293 K) by adjusting the length of the copper plate that was dipped in the liquid nitrogen. Further, it was also possible to increase the sample temperature up to 333 K by simply replacing the liquid nitrogen with hot water. The temperature was monitored by a thermocouple placed right at the sample stage. The chamber was kept under a vacuum to avoid heat transfer from the surrounding atmosphere and to avoid the formation of frost inside the chamber. In order to avoid frost on the optical window, we blew dry nitrogen gas on the outer side of the optical window, as shown in Figure 1a. Although we could not go down to the liquid nitrogen temperature in our cryostat as our cooling was limited by the heat transfer through the copper plate, one of the biggest advantages of our design is that the cryostat is small enough to be mounted on a piezo scanner. The temperature range that we achieved in our system was still good enough for our study. This simple and small cryostat could be efficiently used for Raman imaging, and it sufficiently suppressed the thermal drift for Raman imaging once it was set to a certain temperature.

We constructed an optical setup for Raman measurement underneath our home-built cryostat, as illustrated in Figure 1b. A laser (wavelength: 532 nm, Cobolt, Samba 50) was focused on the sample through an objective lens (NA:0.6, WD:10), and Raman scattered light was collected through the same objective lens in the backscattering geometry. Incident laser

https://dx.doi.org/10.1021/acs.jpcc.0c00416
J. Phys. Chem. C 2020, 124, 6922−6928

power was estimated to be 2 mW at the sample plane. We confirmed that 2 mW of the incident power did not cause any photodamage to our SWCNT sample, where we observed no change in Raman spectra while we kept the SWCNTs irradiated with the incident light for a long time. The exposure time for each Raman spectrum was 0.1 s. The backscattered Rayleigh signal was blocked by a long pass filter that allowed only Raman signal to pass through. The Raman signal was finally detected by a Peltier-cooled charge coupled device (CCD) camera (Teledyne Princeton Instruments, PIXIS: 100_eXcelon) through a spectroscope (HORIBA, HR640). The CCD camera was synchronized with the movement of the piezo scanner for Raman imaging.

3. RESULTS AND DISCUSSION

We performed low-temperature Raman imaging of SWCNTs at different temperatures. The powder of SWCNTs (Nanointegris Inc., IsoNanotubes-S) was dissolved in 1,2-dichloroethane (Wako) and was sonicated for 30 min. A 150 μL portion of the SWCNT solution was spin-casted on a cleaned silicon substrate. The substrate was fixed on the sample stage in the cryostat chamber by a conductive carbon tape. As some examples, parts a–c of Figure 2 show G^+-band intensity images of the SWCNT sample obtained at 333, 292, and 201 K, respectively. Each image was obtained in about 2–3 min, which ensures a negligible amount of sample drift during the imaging. Image sizes are 6 μm × 6 μm with 35 × 35 pixels for all images. As clearly seen, the Raman signal was enhanced as the temperature decreased, which is due to the suppressed anharmonic effect. It should be noted that, although the sample stage drift is sufficiently suppressed during a few minutes of Raman imaging at a certain temperature, the drift could occur when we change the temperature. In order to reduce this drift between the experiments, we made a marker on the sample substrate so that we could readjust the sample position before starting an imaging by locating the marker. This also assured us that even after changing the experimental conditions, such as the temperature, we could always come back to the same SWCNT bundle in every imaging, even if the sample contains many bundles in close proximity to each other. Therefore, we confirm that the images observed in Figure 2a–c are of the same SWCNT bundle. Although the image in Figure 2c is slightly shifted and distorted due to a possible drift in this particular experiment that we could not completely avoid, we still confirmed that the image contained the same bundle that was observed in Figure 2a and b. Figure 2d shows Lorentzian-fitted Raman spectra obtained from the SWCNT bundle observed in Figure 2a–c. Raman peak intensities, shifts, and widths for the G^+-band are calculated through the Lorentzian curve fitting process, which are listed in Table 1 and are also plotted in Figure 1S in the Supporting Information. As expected, with decreasing temperature, the peak intensity of the G^+-band increased, the peak width reduced, and the peak position blueshifted.[16] We would like to note that the position of the G^--band peak, appearing at 1570 cm^{-1}, was randomly changed with respect to temperature. This was not due to the anharmonic effects but due to the low peak intensity that prevented us from performing proper Lorentzian fitting. Although the G^--band should also follow a similar temperature dependence as the G^+-band, we ignore the G^--band, as our fitting is not reliable due to weak intensity of this mode. An advantage of our system based on Raman imaging analysis is that the temperature-dependent Raman spectra can be analyzed from the same SWCNT bundles with a microscale spatial resolution.

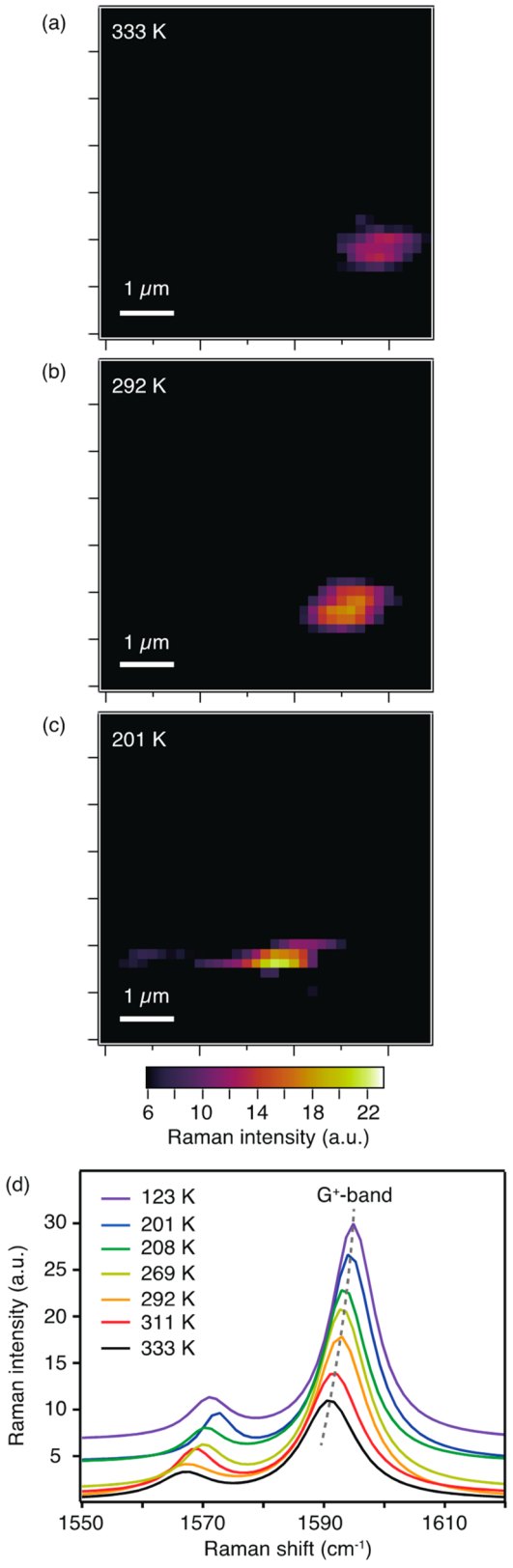

Figure 2. (a–c) Raman images of a SWCNT bundle at temperatures of 333, 292, and 201 K, respectively. (d) Lorentzian-fitted Raman spectra obtained from the same bundle shown in parts a–c at different temperatures.

https://dx.doi.org/10.1021/acs.jpcc.0c00416
J. Phys. Chem. C 2020, 124, 6922–6928

Table 1. Temperature Dependence of Peak Intensity, Peak Position, and Peak Width of the G$^+$-Band, Evaluated from Raman Spectra Shown in Figure 2d

temperature (K)	peak intensity (a.u.)	peak position (cm^{-1})	peak width (cm^{-1})
333	10.7	1590.9	10.9
311	13.0	1591.6	10.8
292	17.4	1592.7	10.5
269	19.4	1593.0	10.0
208	18.7	1593.4	9.2
201	22.4	1594.3	9.2
123	23.2	1594.9	8.7

To investigate the anharmonic effect of individual SWCNT bundles at low temperatures, we further performed temperature-dependent Raman imaging analysis from the sample area shown in the AFM image in Figure 3a. In Figure 3a, several SWCNT bundles are observed, in which the height of the bundles is around 20−30 nm. Figure 3b shows Raman images from the same area obtained at different temperatures ranging from 293 K down to 128 K. These images are constructed by the Raman intensity of the G$^+$-band. Same as in Figure 2a−c, we found that the Raman intensity was enhanced as the temperature decreased. The Raman intensity image taken at 200 K looks a little blurry, which is possibly due to a possible slight defocus of the incident laser. Here, positions 1−3 indicated by the arrows in Figure 3b correspond to positions 1−3 in the AFM image in Figure 3a, respectively. As seen in Figure 3a, positions 1 and 2 are at different locations on the same SWCNT bundle, and position 3 is at another SWCNT bundle. Here, one should note that, while the AFM image shows SWCNT bundles with high spatial resolution, the Raman images are diffraction limited, and hence, they do not show clear shapes of the bundles. Parts c and d of Figure 3 show Raman peak shift images and Raman peak width images, respectively, constructed from the G$^+$-band. A drastic blueshift was observed in the Raman shift images as the temperature reduced. In contrast, a strong change was not observed in the peak width images, although the peak width was indeed sharpened slightly. This could be probably because the lifetime of a phonon depends on many other factors which are temperature-independent. Interestingly, different behaviors in the peak shift and width were observed at each position. For example, position 2 showed drastic frequency shift compared with positions 1 and 3, and the peak width at position 2 was larger than that at the other positions.

Since the changes in the peak shifts are more prominent compared to the change in the peak width, we focused on analyzing the temperature dependence of the Raman shift. Figure 4 shows the temperature dependence of the peak shifts

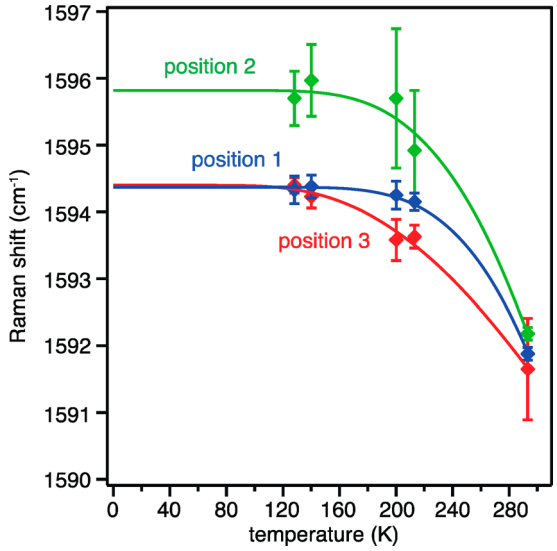

Figure 4. Temperature dependence of the Raman shift of the G$^+$-band at positions 1, 2, and 3, marked in Figure 3a,b.

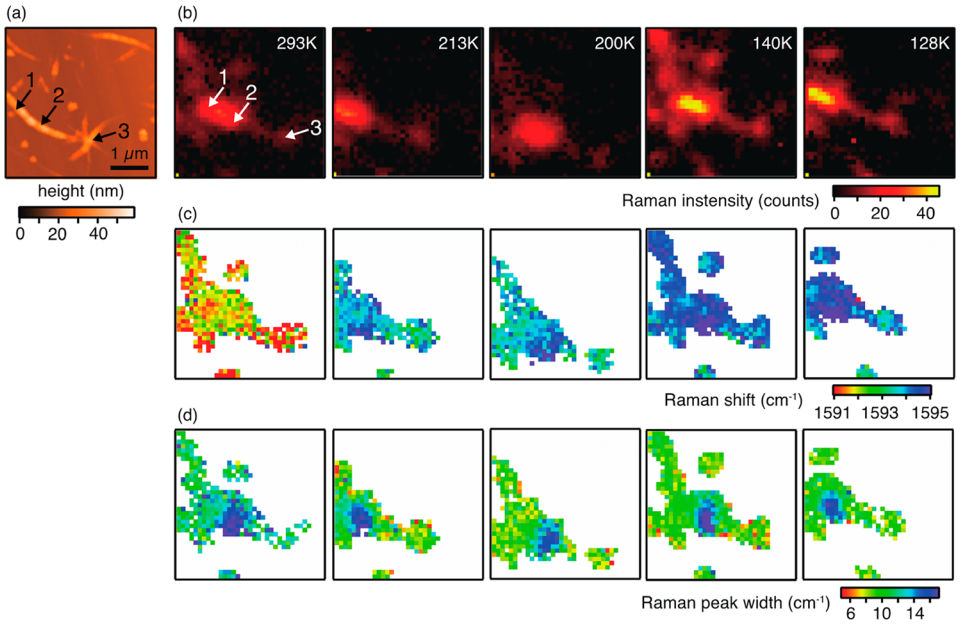

Figure 3. (a) AFM image of SWCNT bundles. (b−d) Raman image from the same area as in part a, constructed from the peak intensity, position, and width of the G$^+$-band, respectively. Temperature was changed from 293 to 128 K. Image sizes are 4 μm × 4 μm for all images.

https://dx.doi.org/10.1021/acs.jpcc.0c00416
J. Phys. Chem. C 2020, 124, 6922−6928

of the G^+-band at positions 1−3, marked in Figure 3a,b. In contrast to some earlier reports on one-point temperature-dependent Raman measurements of SWCNTs, we observed different behaviors of temperature-dependent changes at different locations on different SWCNT bundles in our low-temperature Raman imaging, as seen in Figure 4. According to previous studies on temperature-dependent behavior of Raman scattering,[16,23] Raman shift, $\omega(T)$, that depends on temperature, can be expressed by

$$\omega(T) = \omega_0 - \frac{A}{\exp(B\hbar\omega_0/k_B T) - 1} \quad (1)$$

Here, T is the sample temperature, ω_0 is the original Raman shift at $T = 0$, $\hbar$ is Planck's constant, and k_B is the Boltzmann constant. The parameters A and B are anharmonic constants. The solid lines in Figure 4 are fitted using eq 1. The experimental results agree well with the theory for properly selected values of ω_0, A, and B, which are optimized for the best fitting. Here, a slope region in the higher temperature range and a plateau region in the lower temperature range can be seen in each fitted curve. The slope regions indicate that anharmonic effects gradually reduce as temperature decreases. This also means that, when the slope is steep, the anharmonic effects are stronger. At the same time, the plateau regions indicate that anharmonic effects in this temperature range are weak, and thus, the phonon vibrations are weakly affected by temperature.[7,8] Raman shifts at the plateau regions are different at different positions, which indicates that the effects other than anharmonicity such as bonding strains or defects could also contribute to the Raman shift in SWCNTs. When individual SWCNTs entangle together to form a bundle, they may give rise to bending, stretching, or twisting of individual SWCNTs at the same locations on the bundle. Even point defects, such as an atomic vacancy, may appear during the bundling process. All of these can change the distance or forces between atoms, and thus affect the atomic vibrations of the G^+-mode.[27] Since these structural features are temperature-independent, they become dominant when the dependency on temperature becomes weaker in the plateau region. Therefore, the shift of the plateau region for position 2 in comparison to the other positions indicates increased bundling defects such as strain and other local defects at position 2. As positions 1 and 2 are located on the same SWCNT bundle, it is interesting to observe that our experiments are able to distinguish the change in bundling defects even along a single bundle.

At the slope regions for positions 1 and 2, Raman shifts drastically changed with the temperature as compared to the Raman shift at position 3, indicating stronger anharmonicity at positions 1 and 2, which we believe is due to the bundle effects. As van der Waals interactions between SWCNTs within a bundle interfere with the phonon vibrations of individual nanotubes, it can enhance the anharmonicity in phonon vibrations. Therefore, thicker bundles of SWCNTs can show larger anharmonic effects due to the increased van der Waals interactions. The anharmonicity affecting phonon vibrations due to the intertubular interactions has been reported in a previous study, which also suggested that the intertubular interactions strongly affect the anharmonicity.[14] As estimated from the AFM image in Figure 3a, positions 1 and 2 are located at one thick bundle, whereas position 3 is located at a point where several thinner bundles cross each other. Therefore, in comparison with position 3, quick changes in the Raman shift were observed in the slope regions at positions 1 and 2 in Figure 4 due to the larger anharmonicity arising from the bundle effect. Interestingly, the changes in the Raman shift are slightly different even between positions 1 and 2. The temperature-dependent changes in Raman shift at position 2 are observed to be slightly stronger as compared to those at position 1. This indicates that there could be a slight difference in the bundle effects between positions 1 and 2, even when they are on the same bundle, which cannot be observed through height analysis in the AFM image. Our results suggest that the SWCNTs at position 2 are bundled tighter as compared to those at position 1, inducing larger anharmonicity originating from the bundle effect. This hypothesis is also supported by the fact that the peak shift within the plateau region at position 2 is higher than that at position 1, which could arise due to possible bonding defects and/or stains in the bundle at position 1. Both bonding defects and strains would loosen the bundling of nanotubes, resulting in weaker anharmonic effects at position 1 in comparison with position 2. We deem the larger peak shift in the plateau region at position 2 in comparison with position 1 is also for the same reason.

Our results show that the shift in Raman peak at position 3 is slower with reducing temperature as compared to that at positions 1 and 2. This is because of weak bundle effects, as SWCNTs at position 3 did not form one thick bundle, which can be confirmed from the AFM image in Figure 3a. Rather, a few thinner bundles crossed each other at this location. This organization of SWCNTs in smaller bundles at position 3 induces weaker anharmonicity in phonon vibrations due to the gentle bundle effects as compared to the other two positions. In addition, the Raman shift at the plateau region was low. This shift can be understood from the generation of bonding strains at the crossing points of SWCNT bundles.[24−27] Our home-built Raman imaging system that works at low temperatures enabled us to reveal that the anharmonic effects in SWCNT bundles could be different at different locations, which depends on the nature of the bundling. We were able to investigate the anharmonic effects with a spatial resolution of a few hundred nanometers.

Although the temperature range in our present study is so far limited from 123 to 333 K, we were still able to study the anharmonic effects in SWCNT bundles and their dependence on the bundling effect. In principle, a deeper temperature-dependent analysis of SWCNTs would be preferred for a larger temperature range. The temperature range in our home-built cryostat can be further extended by replacing the media from liquid nitrogen and hot water with liquid helium and hot silicon oil. We believe that the temperature-dependent Raman imaging analysis at a wider temperature range would reveal further details of the thermal properties as well as the anharmonic effects, as we can follow the changes in Raman spectra more precisely, especially at the plateau region of Raman shift at temperatures less than 120 K. Although we have focused our studies on analyzing the G^+-band in the current study, it would also be beneficial to analyze other Raman bands such as RBM and D-band to further understand the thermal properties of SWCNTs as a future prospective.

4. CONCLUSION

We have performed a temperature-dependent Raman imaging analysis of SWCNT bundles, using our unique home-built mini cryostat system. Owing to the spatially resolved Raman

https://dx.doi.org/10.1021/acs.jpcc.0c00416
J. Phys. Chem. C 2020, 124, 6922−6928

imaging analysis, we could investigate individual SWCNT bundles with a spatial resolution of a few hundred nanometers. We revealed that different SWCNT bundles show different behaviors in temperature-dependent Raman scattering. With the aid of an AFM image obtained from the sample that provided the topographic information on SWCNT bundles, we discuss the origin of different behaviors. We found that Raman spectral changes with temperature were different even within the same SWCNT bundle at different locations. Our study not only demonstrates Raman imaging at various temperatures but also reveals how anharmonicity can depend on the bundling of SWCNTs. Further, we discussed the temperature-dependent behaviors in the lower temperature range (plateau region) and in the higher temperature range (slope region) that were interestingly different from one another and provided us some insight about the bundling defects and bundle effects. As we have successfully demonstrated in this work, the temperature-dependent Raman analysis based on spatially resolved imaging will contribute to not only SWCNTs but also any other advanced materials for the fundamental studies of their thermal properties and the anharmonic effects.

■ ASSOCIATED CONTENT

Supporting Information

The Supporting Information is available free of charge at https://pubs.acs.org/doi/10.1021/acs.jpcc.0c00416.

Graphs of peak intensity, shift, and width of G^+-band with respect to temperature, based on data shown in Table 1 (PDF)

■ AUTHOR INFORMATION

Corresponding Author

Prabhat Verma − *Department of Applied Physics, Osaka University, Suita, Osaka 565-0871, Japan;* orcid.org/0000-0002-7781-418X; Phone: +81-6-6879-4710; Email: verma@ap.eng.osaka-u.ac.jp

Authors

Takayuki Umakoshi − *Department of Applied Physics, Osaka University, Suita, Osaka 565-0871, Japan; PRESTO, Japan Science and Technology Agency, Kawaguchi, Saitama 332-0012, Japan*

Masaki Taniguchi − *Department of Applied Physics, Osaka University, Suita, Osaka 565-0871, Japan*

Complete contact information is available at: https://pubs.acs.org/10.1021/acs.jpcc.0c00416

Author Contributions

§T.U., M.T.: These authors contributed equally.

Notes

The authors declare no competing financial interest.

■ ACKNOWLEDGMENTS

This work was supported in part by the JSPS Core-to-Core Program, the Grant-in-Aid for Early-Career Scientists 18K14148, Grant-in-Aid for Scientific Research (A) 19H00870, SECOM Science and Technology Foundation, The Uehara Memorial Foundation, and Shimazu Science Foundation.

■ REFERENCES

(1) Tans, S. J.; Devoret, M. H.; Dait, H.; Thess, A.; Smalley, R. E.; Geerligs, L. J.; Dekker, C. Individual single-wall carbon nanotubes as quantum wires. *Nature* **1997**, *386*, 474−477.

(2) Bachilo, S. M.; Strano, M. S.; Kittrell, C.; Hauge, R. H.; Smalley, R. E.; Weisman, R. B. Structure-assigned optical spectra of single-walled carbon nanotubes. *Science* **2002**, *298*, 2361−2366.

(3) Hone, J.; Batlogg, B.; Benes, Z.; Johnson, A. T.; Fischer, J. E. Quantized phonon spectrum of single-wall carbon nanotubes. *Science* **2000**, *289*, 1730−1733.

(4) Yao, N.; Lordi, V. Young's modulus of single-walled carbon nanotubes. *J. Appl. Phys.* **1998**, *84*, 1939−1943.

(5) Berber, S.; Kwon, Y.; Tománek, D. Unusually high thermal conductivity of carbon nanotubes. *Phys. Rev. Lett.* **2000**, *84*, 4613−4616.

(6) Balkanski, M.; Wallis, R. F.; Haro, E. Anharmonic effects in light scattering due to optical phonons in silicon. *Phys. Rev. B: Condens. Matter Mater. Phys.* **1983**, *28*, 1928−1934.

(7) Verma, P.; Abbi, S. C.; Jain, K. P. Raman-scattering probe of anharmonic effects in GaAs. *Phys. Rev. B: Condens. Matter Mater. Phys.* **1995**, *51*, 16660−16667.

(8) Anand, S.; Verma, P.; Jain, K. P.; Abbi, S. C. Temperature dependence of optical phonon lifetimes in ZnSe. *Phys. B* **1996**, *226*, 331−337.

(9) Bhardwaj, B. S.; Sugiyama, T.; Namba, N.; Umakoshi, T.; Uemura, T.; Sekitani, T.; Verma, P. Orientation analysis of pentacene molecules in organic field-effect transistor devices using polarization-dependent Raman spectroscopy. *Sci. Rep.* **2019**, *9*, 15149.

(10) Bhardwaj, B. S.; Sugiyama, T.; Namba, N.; Umakoshi, T.; Uemura, T.; Sekitani, T.; Verma, P. Raman spectroscopic studies of dinaphthothienothiophene (DNTT). *Materials* **2019**, *12*, 615.

(11) Kato, R.; Umakoshi, T.; Sam, R. T.; Verma, P. Probing nanoscale defects and wrinkles in MoS 2 by tip-enhanced Raman spectroscopic imaging. *Appl. Phys. Lett.* **2019**, *114*, 073105.

(12) Dresselhaus, M. S.; Dresselhaus, G.; Saito, R.; Jorio, A. Raman spectroscopy of carbon nanotubes. *Phys. Rep.* **2005**, *409*, 47−99.

(13) Huang, F.; Yue, K. T.; Tan, P.; Zhang, S. L.; Shi, Z.; Zhou, X.; Gu, Z. Temperature dependence of the Raman spectra of carbon nanotubes. *J. Appl. Phys.* **1998**, *84*, 4022−4024.

(14) Raravikar, N. R.; Keblinski, P.; Rao, A. M.; Dresselhaus, M. S.; Schadler, L. S.; Ajayan, P. M. Temperature dependence of radial breathing mode Raman frequency of single-walled carbon nanotubes. *Phys. Rev. B: Condens. Matter Mater. Phys.* **2002**, *66*, 235424.

(15) Ouyang, Y.; Fang, Y. Temperature dependence of the raman spectra of carbon nanotubes with 1064 nm excitation. *Phys. E* **2004**, *24*, 222−226.

(16) Chiashi, S.; Murakami, Y.; Miyauchi, Y.; Maruyama, S. Temperature dependence of raman scattering from single-walled carbon nanotubes: undefined radial breathing mode peaks at high temperatures. *Jpn. J. Appl. Phys.* **2008**, *47*, 2010−2015.

(17) Zhou, Z.; Dou, X.; Ci, L.; Song, L.; Liu, D.; Gao, Y.; Wang, J.; Liu, L.; Zhou, W.; Xie, S. Temperature dependence of the Raman spectra of individual carbon nanotubes. *J. Phys. Chem. B* **2006**, *110*, 1206−1209.

(18) Zhang, X.; Yang, F.; Zhao, D.; Cai, L.; Luan, P.; Zhang, Q.; Zhou, W.; Zhang, N.; Fan, Q.; Wang, Y.; et al. Temperature dependent Raman spectra of isolated suspended single-walled carbon nanotubes. *Nanoscale* **2014**, *6*, 3949−3953.

(19) Chiashi, S.; Murakami, Y.; Miyauchi, Y.; Maruyama, S. Cold wall CVD generation of single-walled carbon nanotubes and in situ Raman scattering measurements of the growth stage. *Chem. Phys. Lett.* **2004**, *386*, 89−94.

(20) Zhang, L.; Jia, Z.; Huang, L.; O'Brien, S.; Yu, Z. Low-temperature Raman spectroscopy of individual single-wall carbon nanotubes and single-layer graphene. *J. Phys. Chem. C* **2008**, *112*, 13893−13900.

(21) Calizo, I.; Balandin, A. A.; Bao, W.; Miao, F.; Lau, C. N. Temperature dependence of the raman spectra of graphene and graphene multilayers. *Nano Lett.* **2007**, *7*, 2645−2649.

(22) Maher, R. C.; Cohen, L. F.; Gallop, J. C.; Le Ru, E. C.; Etchegoin, P. G. Temperature-dependent anti-stokes/stokes ratios under surface-enhanced Raman scattering conditions. *J. Phys. Chem. B* **2006**, *110*, 6797−6803.
(23) Cui, J. B.; Amtmann, K.; Ristein, J.; Ley, L. Noncontact temperature measurements of diamond by Raman scattering spectroscopy. *J. Appl. Phys.* **1998**, *83*, 7929−7933.
(24) Fuhrer, M. S.; Nygård, J.; Shih, L.; Forero, M.; Yoon, Y. G.; Mazzoni, M. S. C.; Choi, H. J.; Ihm, J.; Louie, S. G.; Zettl, A.; et al. Crossed nanotube junctions. *Science* **2000**, *288*, 494−497.
(25) Shan, B.; Lakatos, G. W.; Peng, S.; Cho, K. First-principles study of band-gap change in deformed nanotubes. *Appl. Phys. Lett.* **2005**, *87*, 173109.
(26) Okuno, Y.; Saito, Y.; Kawata, S.; Verma, P. Tip-enhanced Raman investigation of extremely localized semiconductor-to-metal transition of a carbon nanotube. *Phys. Rev. Lett.* **2013**, *111*, 216101.
(27) Yano, T.; Ichimura, T.; Kuwahara, S.; Dhili, F. H.; Uetsuki, K.; Okuno, Y.; Verma, P.; Kawata, S. Tip-enhanced nano-Raman analytical imaging of locally induced strain distribution in carbon nanotubes. *Nat. Commun.* **2013**, *4*, 2592.

https://dx.doi.org/10.1021/acs.jpcc.0c00416
J. Phys. Chem. C 2020, 124, 6922−6928